Hindawi
Advances in Civil Engineering
Volume 2023, Article ID 2427773, 13 pages
https://doi.org/10.1155/2023/2427773

Research Article

Field-Scale Experimental Study on Thermomechanical Behaviors of Super-Long and Large-Diameter Energy Piles under Liquefied Natural Gas Tank

Li Xiao,[1] Chao Zhang,[1] Yang Liu,[1] Mingrui Zhao,[1] Guangzhe Zhang ,[2,3] Fenglei Du,[2,3] Xiangyu Li,[2,3] and Dongjian Yu[2,3]

[1]*CNOOC Gas and Power Group, Block C, CNOOC Building, Yard 6, Taiyanggong South Street, Beijing 100028, China*
[2]*Institute of Foundation Engineering, China Academy of Building Research, Beisanhuan East Road No. 30, Beijing 100013, China*
[3]*State Key Laboratory of Building Safety and Environment, China Academy of Building Research, Beisanhuan East Road No. 30, Beijing 100013, China*

Correspondence should be addressed to Guangzhe Zhang; guangzhe_zhang@hotmail.com

Received 8 October 2022; Revised 21 December 2022; Accepted 2 May 2023; Published 3 August 2023

Academic Editor: Sudip Basack

In this work, field-scale experiments were carried out on two energy piles to investigate the mechanical behavior of the piles when subjected to thermomechanical loads under a liquefied natural gas tank. The results showed that the super-long and large-diameter energy pile exhibited a better heat transfer performance. After pile heating or cooling, the temperature in the mid-depth of the pile increased or decreased rapidly, and at the two ends, the temperature varied relatively slowly. Regarding the observed axial strain, energy pile 1 exhibited predominately compressive deformation during the coupled heating–loading process, while a certain tensile deformation was found near the pile toe of energy pile 2 during the coupled cooling–loading process. Moreover, for both energy piles, positive shaft resistances appeared predominately under both the pure mechanical and coupled thermomechanical conditions, and occasional and local occurrences of negative resistances could be related to the ground conditions on site. The settlement and bearing capacity values of the two energy piles were not significantly affected by the coupled thermomechanical loads, and thus, the serviceability of the gas tank would not diminish.

1. Introduction

Piles as a kind of deep foundations are slender columns made of materials like steel or concrete, and used to support the superstructure and transfer the loads at desired depth by either skin friction or end bearing. Over the years, various types of piles have been designed in consideration of their characteristics and general uses, such as steel piles, concrete piles, cement fly-ash gravel (CFG) piles, stiffened deep cement mixing (SDCM) piles. These piles are predominately loaded axially and/or transversely under different geological conditions (e.g., earthquake) and artificial influences (e.g., explosion). The evaluation of workability, serviceability, and stability of the pile is therefore of vital importance in civil engineering [1–4].

Compared to the use of a traditional ground source heat pump (GSHP), the use of shallow geothermal energy can also be realized by an energy pile, because concrete has a better thermal conductivity than soil [5]. Energy piles can not only be used for supporting superstructures but also for cooling and heating buildings. However, whether thermal loads associated with structural loads changing the initial interaction between the pile and soil, and further on affecting the safety of the pile are unknown. For this reason, in the last two decades, studies on the mechanical behaviors of energy piles subjected to separate and coupled thermomechanical loads under different ground conditions (e.g., sand, silt, and clay) have been performed by many scholars through in situ full-scale experiments [6–21], small-scale model tests [22–30], and numerical analyses [31–36].

Regarding the field-scale experiments, Laloui et al. [6] found that the strain of an energy pile after one loading and heating cycle was thermoelastic. The intensity was

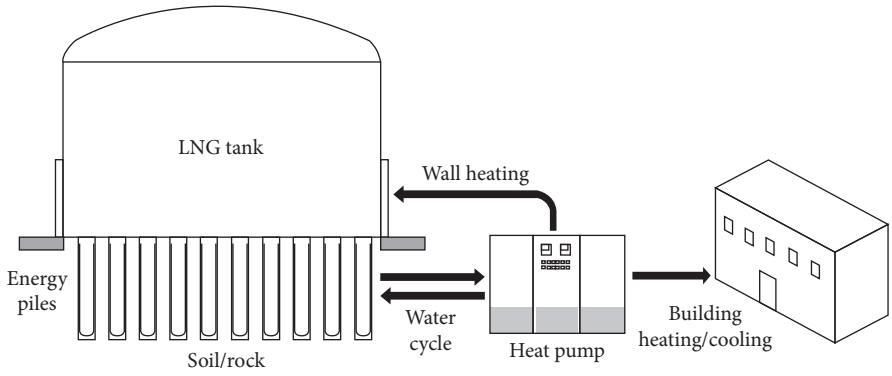

Figure 1: Application of energy pile system in petroleum and chemical industry.

mainly dependent on the types of the surrounding soils. Sutman et al. [11] reported that the pile expansion was restrained by the surrounding soils on the sides and at the pile toe. These restricted strains generated by the temperature increased during heating, resulting in compressive axial stresses along the pile. Amatya et al. [8] discussed the changes of the axial stresses and mobilized shaft resistances of energy piles in response to heating and cooling, and they pointed out that the change of the pile–soil interaction could be attributed to the ground conditions, end restraints, and thermal load. Gui and Cheng (2014) [14] emphasized that additional thermal stresses (compressive and tensile stresses) during the heating and cooling processes associated with mechanical stresses could exceed the ultimate bearing capacity of the pile, which needs to be considered more carefully for the structural design of energy piles. You et al. [15] pointed out that, in the cooling case, a thermally induced tensile axial stress superimposed with the initial mechanical compressive stress became the total compressive or tensile stress. The tensile stress could be generally induced at the lower part of the pile. The results of Murphy et al. [10] showed that, for a temperature increase of 18°C, the maximum thermal axial stress ranged from 4.0 to 5.1 MPa, and the maximum upward displacement (heave) was in the range of 1.4–1.7 mm. Wang et al. [13] found that the bearing capacity of the pile increased after the pile was heated, and then, it returned to the initial capacity after the pile naturally recovered to the initial temperature. The authors drew the following conclusion: There was no loss in the pile shaft capacity after the heating and cooling cycles, which confirmed the previous conclusions that the pile exhibited a thermoelastic behavior. Faizal et al. [18] studied both the axial and radial thermal responses of energy piles to monotonic and cyclic temperature changes. The authors found that under a constant structural load, cyclic thermal loads caused a reversible thermal response at the pile–soil interface. Previous studies indicated that an energy pile expands or contracts when it is heated or cooled. This changes the initial interaction between the pile and soil (e.g., strain, stress, and shaft resistance) and may result in additional settlement and deterioration of the bearing capacity of the pile.

In this work, based on a pilot project, field-scale experiments were carried out to study the mechanical behaviors of two energy piles that underwent separate and coupled thermomechanical loads under a liquefied natural gas (LNG) tank. As shown in Figure 1, since the energy pile system is being applied for the first time in the petroleum and chemical industry, the structural design of the energy piles has priority. The aim of this work is to ensure that when the temperature changes within a certain range, the geotechnical analysis of the pile indicates that the additional settlement and the bearing capacity do not exceed the allowable values so that the serviceability of the tank will not diminish. Moreover, the heat transfer performances of energy piles were also evaluated and then compared with those of previous studies. The results of this work can provide basic knowledge and serve as a preliminary reference for the practical application of super-long and large-diameter energy piles under an LNG tank.

2. Materials and Methods

The pilot project was located at the shoreside of the Yangtze River in the city of Wuhu, in the Anhui province of China, as shown in Figure 2. According to the geological survey conducted on the site, the soil strata included the Holocene marine sediments, the Upper Pleistocene lacustrine and marine sediments, and the Upper Pleistocene marine and continental alternated Quaternary sediments. The ground was composed mainly of three sedimentary types of soils: clay, sand, and sandstone. The detailed distribution of the soil is shown in Figure 3. Moreover, two types of groundwater were identified in this site. The perched groundwater was distributed in the fill material layer, and the confined groundwater was distributed in the silty to gravelly sand layers. The confined groundwater was well connected with the Yangtze River, which means that the confined groundwater varied with the water table of the Yangtze River, and its value was measured at about 3.2–4.4 m below the ground surface during the surveying.

The designed cast-in-place concrete pile was 53 m in length and 1.2 m in diameter. The main part of the pile was placed in the sand layer (i.e., silty to gravelly sand), and the pile toe was inserted into the moderately weathered sandstone. The reinforcing cage had a diameter of 1 m and extended the full length of the pile. The designed 3U-shaped polyethylene (PE) tube with a total length of about 250 m was

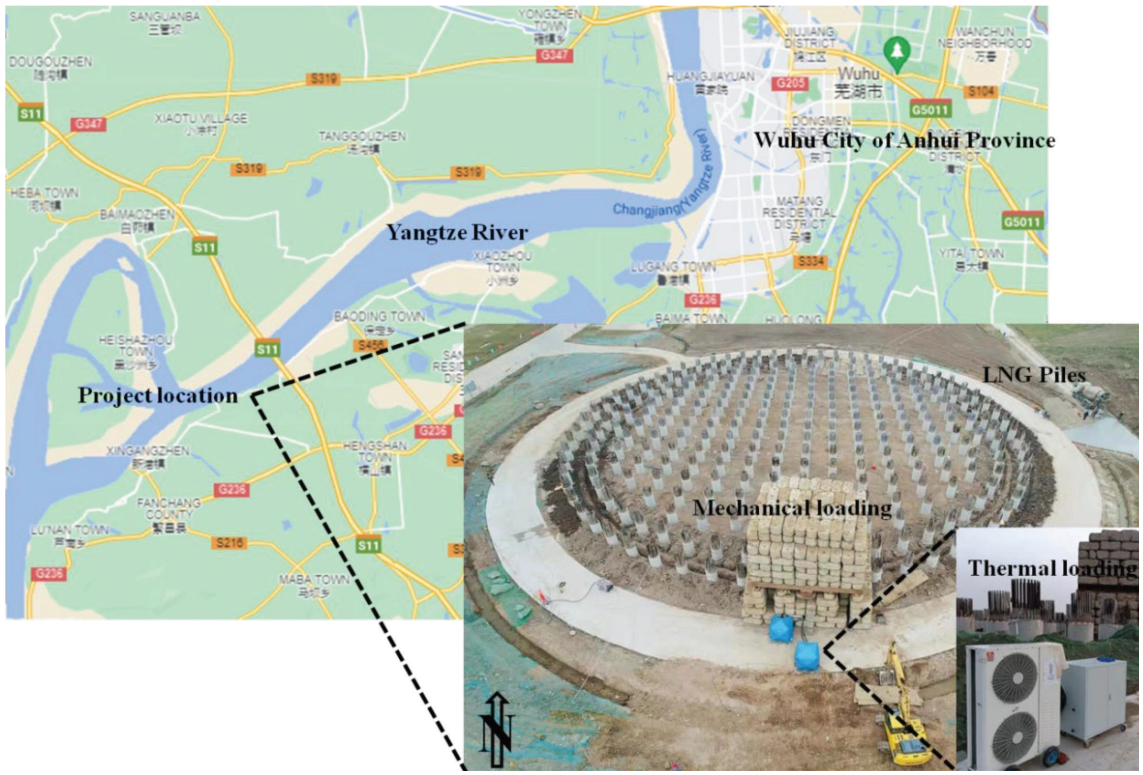

FIGURE 2: Location of pilot project location and construction of energy piles.

attached to the inside of the reinforcing cage. The inner and outer diameters of the tube were 26 and 32 mm, respectively. According to the soil strata on site and the pile length, eleven vibrating wire strain gauges (VWSGs) were installed in the pile to measure the axial strain and temperature at various depths. The detailed positions of the VWSGs are shown in Figure 3.

Static load tests were carried out according to the China Industry Standard JGJ 106-2014 [37]. Since the designed maximum load was set to 11,000 kN, nine levels of working loads were applied stepwise to press the pile. The corresponding displacements of the pile were measured using two linear variable differential transformers (LVDTs), which were positioned on the pile top.

Due to special application of the LNG tank, two individual experiments were designed in order to better reflect the realistic working behaviors of the energy piles under the LNG tank. First, static loads without any thermal loads were imposed on the two energy piles (EPs) separately to simulate the loading process of the pile caused by the storage (filling and emptying) of LNG. After that, the two EPs were heated and cooled, and they simultaneously experienced mechanical loads to examine the response of the pile to coupled thermomechanical loads. The detailed experimental design is shown in Figure 4. EP1 was used as a heating pile, and EP2 was used as the cooling pile. During the test, the measured data were the inlet and outlet fluid (normal water) temperatures, the fluid flow rate and the heating or cooling power in the thermal response test (TRT) unit, the axial strain and temperature at different depths of the pile, and the working load and the corresponding displacement (heave or settlement) at the pile top. Figure 5 shows the construction of the EP on site.

3. Results

3.1. Heat Transfer Performance. Figures 6(a) and 6(b) show the inlet and outlet water temperatures recorded by the TRT unit, as well as the temperature difference calculated by subtracting the outlet water temperature from the inlet temperature for heating EP1 and cooling EP2, respectively. When EP1 was heated, the temperature began to rise immediately and continuously, and at the end of heating process, the inlet and outlet water temperatures were measured at 37.9 and 33.4°C, respectively. Similarly, when EP2 was cooled, the temperature began to decline with time, and at the end of the cooling process, the inlet and outlet water temperatures were measured at 7 and 9.3°C, respectively. Laloui et al. [6] reported that a temperature difference of about 2°C between the fluid inflow and outflow from the primary circuit is sufficient for the economical operation of an energy system. In this work, temperature differences of about +4.5°C for EP1 and −2.3°C for EP2, respectively, were obtained between the inflow and outflow water.

Based on the temperature data, the heat flux was calculated using the following equation:

$$Q = \rho_{\text{Fluid}} C_{\text{Fluid}} V (t_{\text{in}} - t_{\text{out}}), \quad (1)$$

where Q (in watts) denotes the heat flux, ρ_{Fluid} (in kilograms per cubic meter) is the mass density of the fluid, which is

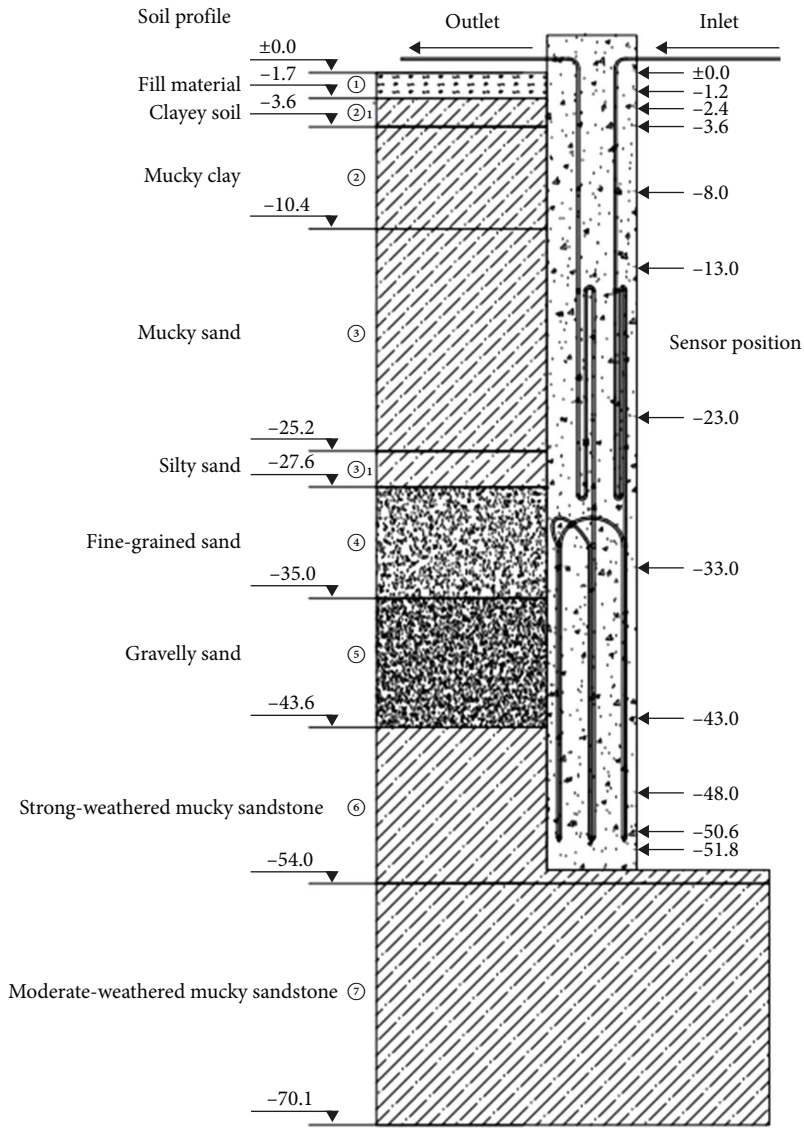

FIGURE 3: Soil profile and instrumentation of the pile.

1,000 kg/m^3 for normal water, C_{Fluid} (in joules per kilogram degree celcius) is the specific heat capacity of the fluid, which is 4.2×10^3 J/kg°C for normal water, V (in cubic meters per hour) is the fluid flow rate, which was fixed at 1.8 m^3/hr in this work, and t_{in} and t_{out} (in degree celcius) are the inlet and outlet water temperatures, respectively. The corresponding heat flux was calculated as follows:

$$q = \frac{Q}{L}, \tag{2}$$

where q (in watts per meter) denotes the heat transfer rate, and L is the effective pile length.

When the outlet water temperature was set at 38°C for heating EP1 and the temperature difference between the inlet and outlet water in the quasi-stable state was found to be about 4.5°C, the heat flux of the pile was calculated to be 9.5 kW, and the corresponding heat transfer rate was 178.3 W/m. The outlet water temperature was set to 7°C for cooling EP2. At the end of the cooling process, when the temperature difference was stabilized at about 2.3°C, the heat flux and heat transfer rate of the pile were determined to be 4.8 kW and 91.1 W/m, respectively.

3.2. Temperature Distribution. Figure 7(a) shows the temperatures distributed along EP1 after pile heating. At the initial state, the ground temperature decreased with depth: The highest temperatures (26.4, 25.9, and 27.1°C) were measured at the upper parts of the pile (−1, −3, and −4 m), the temperatures (22.8−23.5°C) in the middle parts of the pile (−8 to −23 m) were less than those in the upper parts, and the lowest temperatures (20.4−21.0°C) were observed at the lower parts of the pile (−43 to −51 m). After switching on the heat pump, the temperatures of the pile shaft begin to rise, and at the end of the heating process, the temperatures measured at −1, −3, and −4 m were 27.6, 27.4, and 28.7°C, respectively, which showed that the changes were small

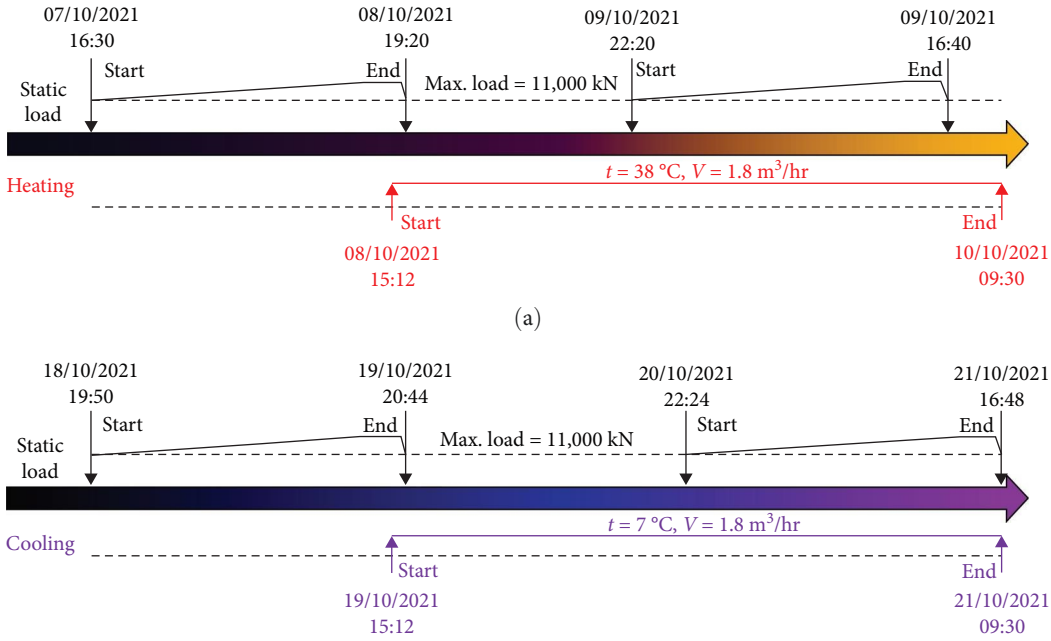

Figure 4: Experimental design. (a) Energy pile 1 (heating pile). (b) Energy pile 2 (cooling pile).

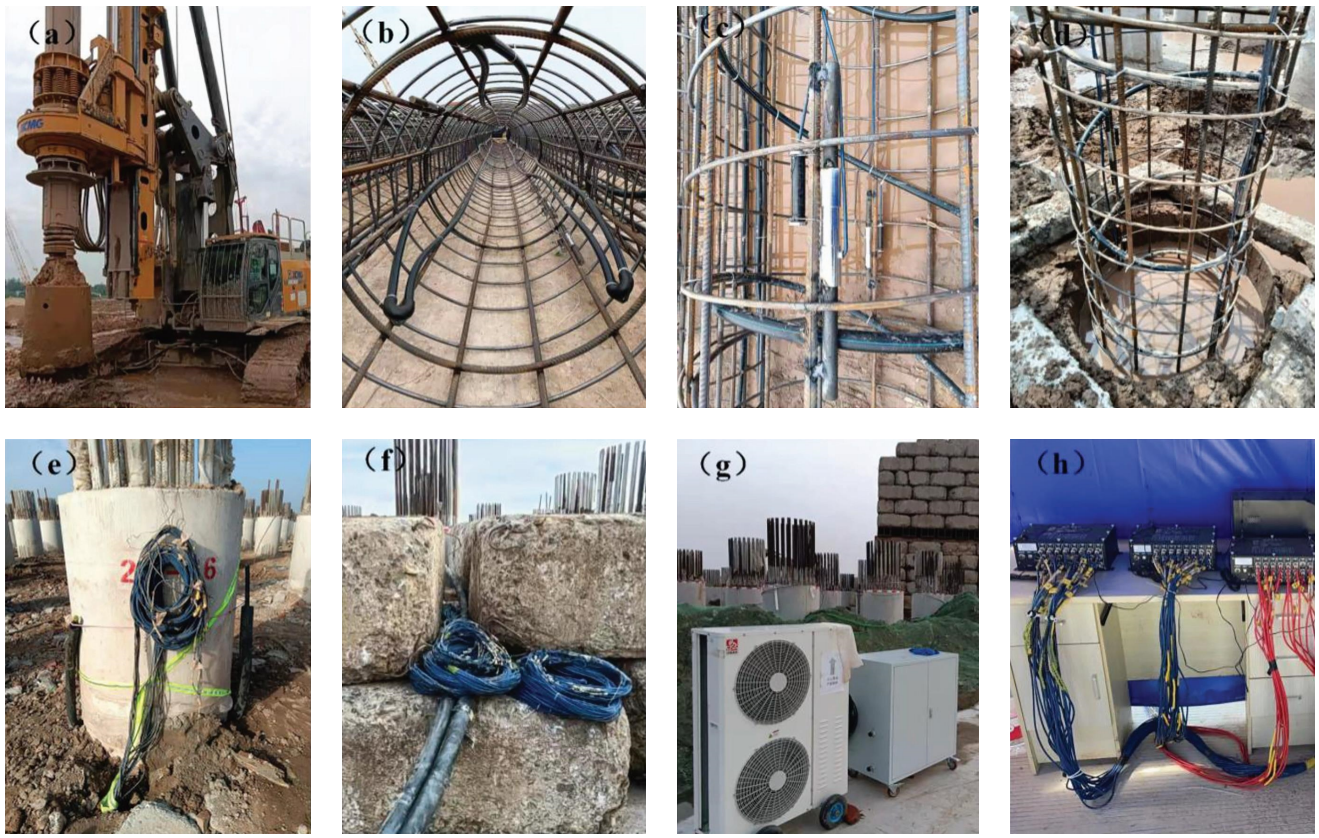

Figure 5: Construction of energy pile on site: (a) borehole drilling; (b) reinforcing cage with 3U-shaped tube; (c) sensor instrumentation; (d) burying of reinforcing cage; (e) pile after cast-in-place concrete ready for test; (f) stacking of concrete blocks for static load test; (g) applied apparatus for thermal response test; (h) data measurement of strains and temperatures.

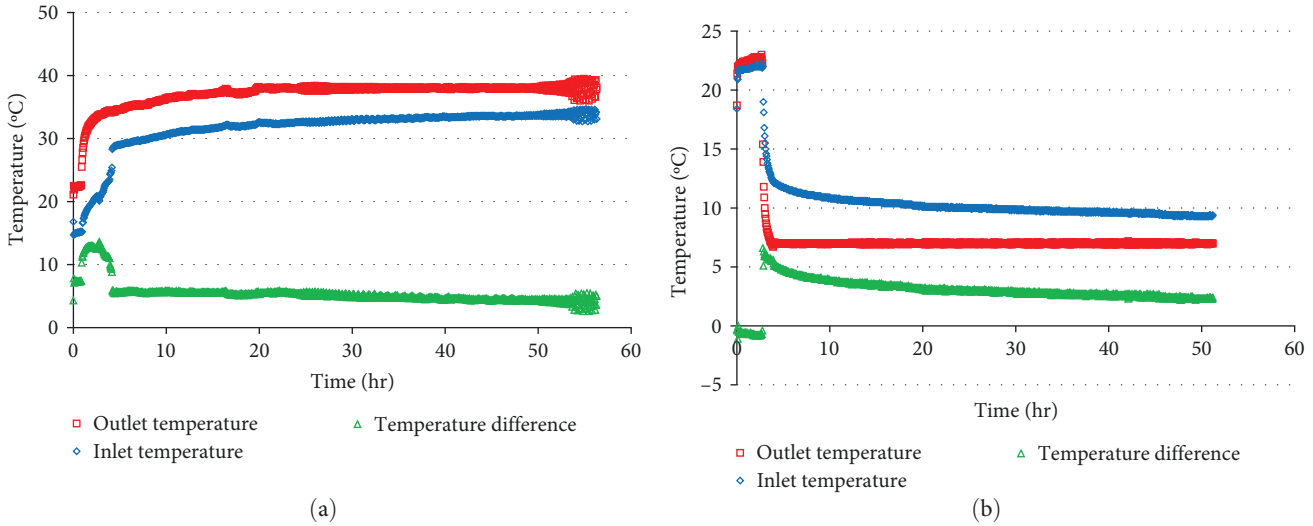

Figure 6: Evolution of inlet and outlet water temperatures with time. (a) Energy pile 1 (heating pile). (b) Energy pile 2 (cooling pile).

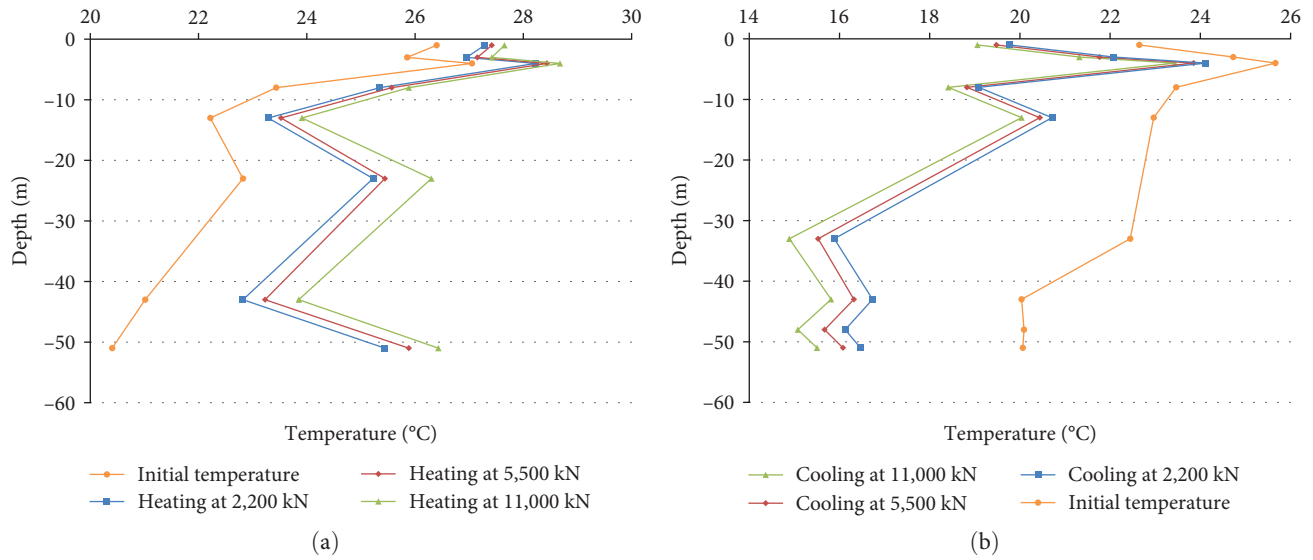

Figure 7: Temperature variations with depth. (a) Energy pile 1 (heating pile). (b) Energy pile 2 (cooling pile).

compared to the initial state. It was reasonable to assume that the temperatures in the upper parts of the pile were affected by the atmospheric temperature. The temperature in the middle parts of the pile (i.e., −23 m) increased from 22.8 to 26.3°C, and the corresponding temperature difference was about 3.5°C. The largest temperature difference of about 6.0°C was found at the pile toe (i.e., −51 m). This may have been because the sensors were placed relatively close to the hot water tube at this position. Fang et al. [21] emphasized that the temperature was sensitive to the distance of the sensor from the heat exchanger: The closer the sensor was to the heat exchanger, the higher the measured temperature was. Figure 7(b) shows the temperature distribution along EP2 after pile cooling. Similar to EP1, the initial ground temperatures decreased gradually with depth. The highest temperature was also found near the pile top (e.g., 25.7°C at −4 m) due to the ambient temperature. During the cooling process, the temperature of the pile began to decline. The temperatures in the middle parts of the pile decreased rapidly, while at the two ends, they decreased slowly. In summary, at the stages of pile heating and cooling, the temperature changes for the two EPs were similar: The temperature in the mid-depth of the pile increased or decreased rapidly, and at the two ends of the pile, the temperatures changed slowly.

3.3. Observed Axial Strain. The observed axial strain (ε_{Obs}) measured by the VWSGs needed to be corrected for the temperature effects due to pile heating or cooling. The formula is as follows:

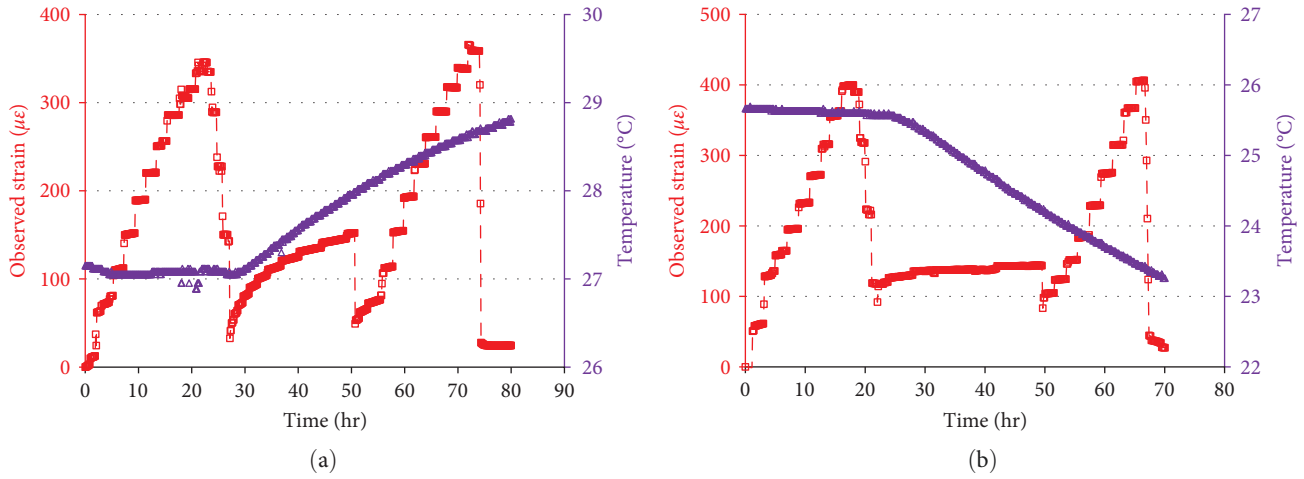

FIGURE 8: Evolution of temperatures and observed strains with time at a depth of −4 m. (a) Energy pile 1 (heating pile). (b) Energy pile 2 (cooling pile).

$$\varepsilon_{\text{Obs}} = (f_i^2 - f_0^2)GB + (T_i - T_0)\alpha_s, \tag{3}$$

where f_i is the resonant frequency of the strain gauges at time i, f_0 is the reference resonant frequency of the strain gauges, GB is the calibration factor of the strain gauges, where G is the gauge factor and B is the batch factor, T_i is the temperature of the strain gauges at time i, T_0 is the reference temperature of the strain gauges, and α_s is the coefficient of linear thermal expansion of the steel wire in the strain gauges (12.2 $\mu\varepsilon$/°C). Note that the value of f_0 was selected at the beginning of each experiment to remove the effects of any strains due to self-weight of the pile and curing of the concrete. The use of this equation assumes that the temperature of the steel wire was the same as that of surrounding reinforced concrete, which should be valid for seasonal temperature fluctuations, but it may not be valid for more rapid temperature fluctuations of several days due to the insulating effect of the air surrounding the steel wire within the VWSG casing [9].

The measurement data recorded by the sensors placed at the depth of −4 m are considered as sample data. The violet line in Figure 8(a) indicates the evolution of the temperature for EP1 during the pure mechanical and coupled thermomechanical processes. It is clear that the temperature at the pure mechanical stage was kept almost unchanged at 27.1°C. After pile heating, the temperature increased continuously, and at the end of the heating process, the temperature reached 28.7°C. Moreover, the red line in Figure 8(a) indicates the evolution of the ε_{Obs} at −4 m for EP1. The results showed that the observed strains measured at each load level during the coupled heating and loading process were higher than those during the pure mechanical loading process, which means that the pile expanded when it was heated. The violet line in Figure 8(b) shows that the initial temperature within EP2 had a more or less constant value of 25.7°C in the pure mechanical stage, and this value was reduced to 23.3°C at the end of the cooling process. The red line in Figure 8(b) shows that the observed strains at the end of the first and second loading processes were more or less equal to each other for EP2, which means that the cooling effect could play a certain role.

Figure 9 shows the ε_{Obs} along EP1 and EP2 before and after pile heating and cooling at the load levels of 2,200, 5,500, and 11,000 kN. In the pure mechanical stage, two conclusions can be obtained based on the dashed lines in Figure 9: (1) At the same load level (e.g., 2,200, 5,500, or 11,000 kN), the observed strain decreased with depth, and its value was almost zero at the pile toe, and (2) at the same depth, as the working load increased (e.g., from 2,200 to 5,500 and then to 11,000 kN), the mechanically induced strain increased. These behaviors reflect the working behavior of a friction pile. Figure 9(a) compares the observed strains before and after heating EP1. The results showed that, at the same load level, the observed strain increased slowly with increasing temperature, which reflected the characteristics of pile expansion due to heating. The solid lines in Figure 9(b) show the change of the observed strains with depth for EP2 after pile cooling. The observed strain was mainly governed by the mechanical load. When the working load was relatively low (e.g., 2,200 and 5,500 kN), the temperature change at each load level was relatively small. However, at the end of the coupled cooling and loading process (e.g., 11,000 kN), the observed strain along the pile was lower than that in the initial state, which indicated that the pile contracted when it was cooled. It is worth noting that the temperature decrease, during cooling, caused the contraction of the upper and lower parts of the pile relative to the neutral point when the two ends of the pile were free. In this work, the upper parts of EP2 represented compressive deformation due to loading on the pile top, while a certain tensile deformation was found near the pile toe, which might have been due to the existence of collapsed sediments (e.g., sand) at the bottom of the pile, indicating a relatively free end restraint.

3.4. Mobilized Shaft Resistance. It is well known that when a pile is loaded axially, the axial strain has the highest value at the pile top, and this value decreases with depth as the shaft resistance is mobilized at the pile–soil interface. The axial

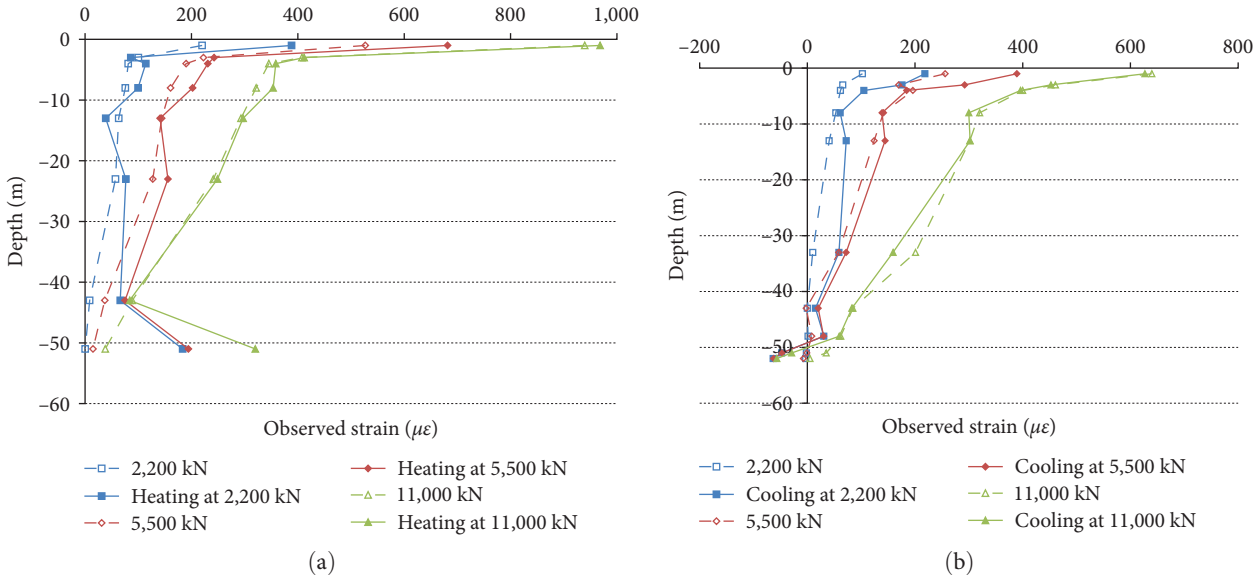

Figure 9: Variations of observed strains with depth. (a) Energy pile 1 (heating pile). (b) Energy pile 2 (cooling pile).

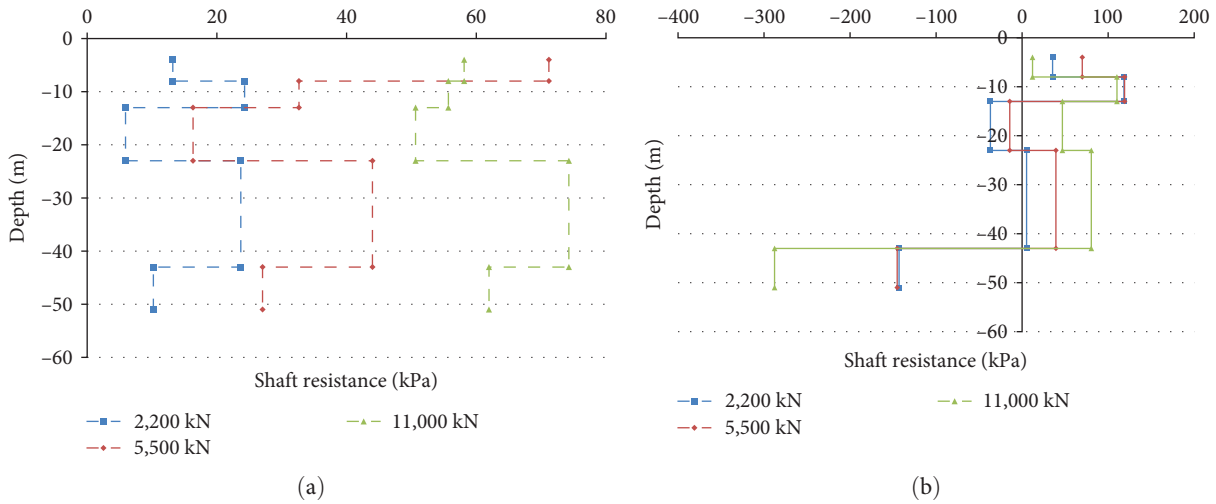

Figure 10: Distributions of mobilized shaft resistances along energy pile 1. (a) Before heating. (b) After heating.

strain will decrease to zero if the shaft resistance is sufficient against the upper load; if not, it will decrease to a nonzero value, and the end bearing resistance will then be mobilized at the pile toe. The mobilized shaft resistance is calculated as follows:

$$f_{\mathrm{mob},i} = \frac{\left(P_{T,i-1} - P_{T,i}\right)}{A_i}, \tag{4}$$

where $f_{\mathrm{mob},i}$ is the mobilized shaft resistance, $P_{T,i-1}$ and $P_{T,i}$ are the mechanical loads imposed on sections i_1 and i, respectively, and A_i is the lateral area i of the pile.

Figure 10 shows the shaft resistance mobilized along EP1 during the pure mechanical and coupled thermomechanical processes. As shown in Figure 10(a), when EP1 was not heated, the shaft resistance exhibited an irregular distribution with depth at the same load level (e.g., 2,200, 5,500, or 11,000 kN). When the applied load was increased (e.g., from 2,200 to 5,500 and then to 11,000 kN), it is reasonable to assume that the positive resistance was predominately mobilized and increased with increasing load. During the coupled heating and loading process, the mobilized shaft resistance in Figure 10(b) also showed an irregular distribution with depth, and the shaft resistance showed an increasing trend with increasing load. The upper load had a positive effect on the reduction of the negative shaft resistance due to pile heating. It is noteworthy that a high negative shaft resistance was identified at the pile toe, which may have been due to the existence of collapsed sediments (e.g., sand) at the bottom of the pile. This confirmed the results of Lu et al. [17], who found that negative shaft resistances occur at different parts

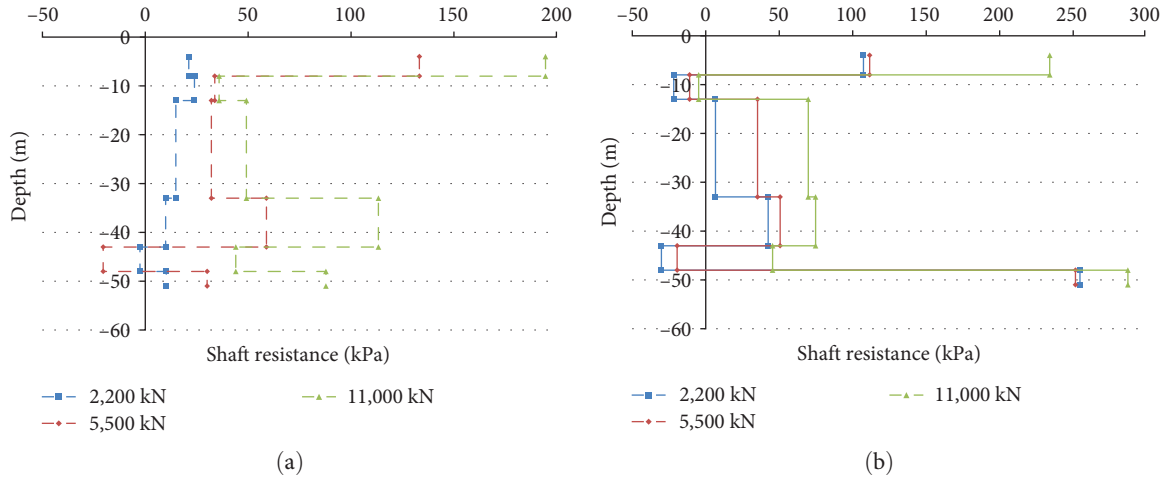

Figure 11: Distributions of mobilized shaft resistances along energy pile 2. (a) Before cooling. (b) After cooling.

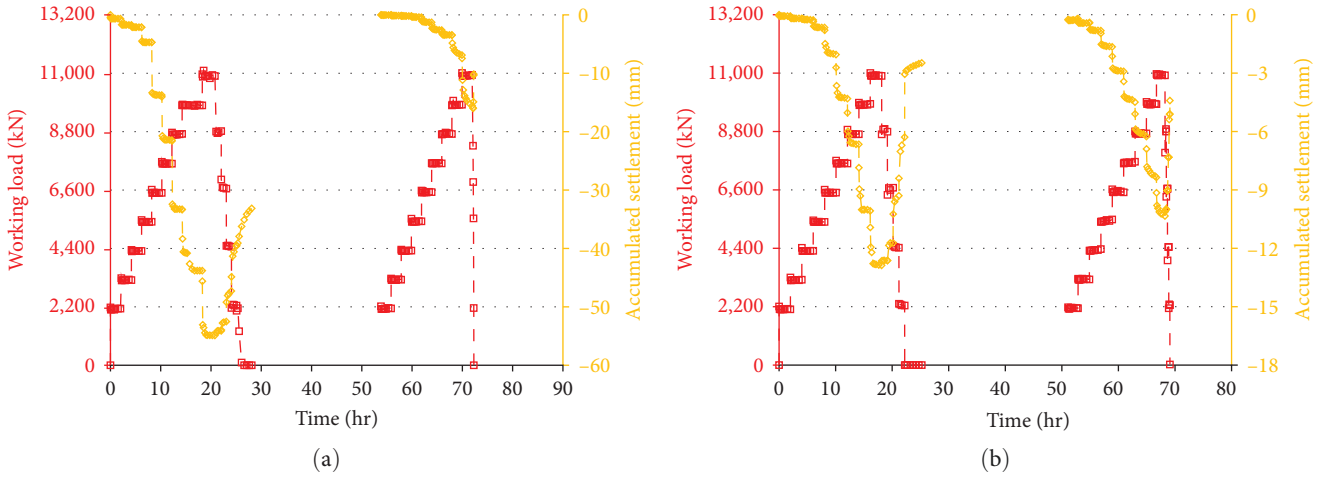

Figure 12: Evolution of load and settlement values with time. (a) Energy pile 1 (heating pile). (b) Energy pile 2 (cooling pile).

of the pile shaft after heating, and these values decrease when the applied loads are increased.

Figure 11 compares the mobilized shaft resistances at various depths before and after cooling EP2. During the pure mechanical process, positive mobilized shaft resistances occurred predominately and became greater with increasing load. The occurrence of negative resistances can be attributed to the properties of the surrounding soil. During the coupled cooling and loading processes, the shaft resistances also showed an increasing trend with increasing load, and negative resistances occurred occasionally and locally. The high shaft resistances may have been due to an issue in the responses of the VWSGs to the temperature changes. It is worth noting that groundwater seepage could also change the interactions between the pile and soil, which might be good for the structural response of the pile.

3.5. Pile Settlement and Bearing Capacity. Figure 12 shows the applied working load and the induced pile displacement plotted against to the corresponding time for EP1 and EP2, respectively. A negative displacement corresponded to pile settlement. It is reasonable to conclude that the settlement values of the two EPs increased with increasing load and decreased with decreasing load. For EP1 at the pure mechanical stage, the cumulative settlement reached 54.9 mm at the end of loading process and then recovered to 33.2 mm at the end of the unloading process. This relatively high settlement could be attributed to the consolidation of collapsed sediments (e.g., sand) at the bottom of the pile. During the coupled heating and loading process, when the maximum load of 11,000 kN was reached again, the accumulated settlement was measured at 15.9 mm, which was about 29.0% of the initial state, and after the pile was totally unloaded again, the accumulated settlement was reduced to 10.2 mm, which was 30.7% of the initial state. These behaviors reflected the fact that heating could reduce the pile settlement. The cumulative settlement at the pile top of EP2 was measured to be 12.9 mm at the end of the first loading process and 2.48 mm at the end of the unloading process. During the cooling process, the accumulated settlement values were then found to be 10.3 and 4.4 mm at the end of second loading and unloading processes, respectively, which were 80.3% and

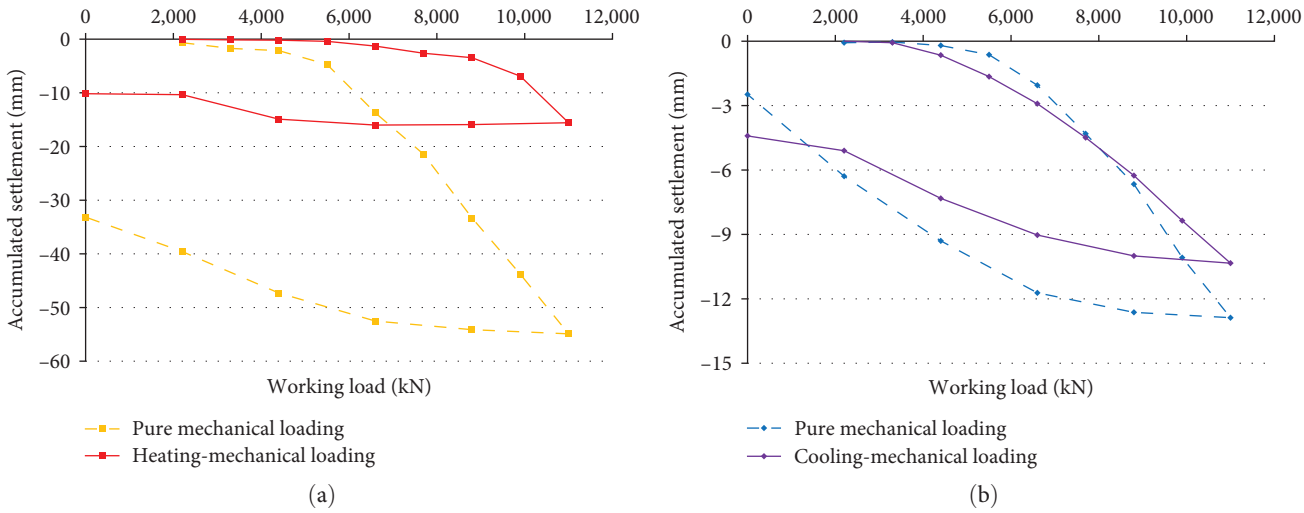

Figure 13: Load–settlement curves. (a) Energy pile 1 (heating pile). (b) Energy pile 2 (cooling pile).

177.8% of the initial states. The increased residual settlement indicates that cooling could cause additional and irreversible settlement of the pile. According to JGJ 106-2014 [37], if the load–settlement (Q–s) curve varied gently, the total settlement of the pile could reach 60–80 mm, and if the end bearing resistance was not completely mobilized, the pile could be loaded until the total settlement at the pile top reached more than 80 mm. In this work, according to the test results, the settlement of the two EPs did not exceed the allowable settlement.

Figure 13(a) compares the Q–s curves of EP1 in the pure mechanical stage and in the coupled heating and loading stage. When the maximum load of 11,000 kN was reached, the total settlement values of the pile were found to be 54.9 and 15.6 mm before and after heating, respectively. The negative slope of the Q–s curve after pile heating was much smaller than that before pile heating, and the settlement was also smaller than that before the pile heating, especially with the gradual increase in the load. The pile settlement significantly decreased after pile heating, meaning that the bearing capacity of the pile was improved. As shown in Figure 13(b), under both the pure mechanical and the coupled thermomechanical conditions, the Q–s curves did not show a significant difference, which means that the bearing capacity of EP2 did not change significantly due to pile cooling in this work.

4. Discussion

Previous studies [31–36] indicated that the heat transfer performance of an EP expressed by the heat flux and heat transfer rate can be affected by many factors, such as the inlet fluid temperature and velocity, the types of soils and their thermal properties, including their conductivities and heat capacities, the pile length and diameter, and the shapes and lengths of the installed PE tubes. A comparison of the heat transfer performances from different studies is shown in Table 1. Most piles had lengths of 10–30 m, so that the heat transfer performance might be limited within a certain range. Overall, the length and diameter increase of the pile could enlarge the heat transfer area and thus improve the heat transfer rate. According to the test results, we can deduce that the super-long and large-diameter EP will have a better heat transfer performance. Moreover, the heat diffusion could be related to the ground conditions. When clayey or silty soils with low permeability existed, the heat exchange between the pile and soil was mainly in the form of heat conduction. However, when the soils were highly permeable sand or gravel, the heat exchange was mainly via heat convection. It should be noticed that the groundwater seepage on site is another important factor affecting the temperature distribution along the pile, as well as the heat transfer performance of the pile [38]. Groundwater seepage can reduce the temperature difference, which is beneficial to the heating or cooling balance of the pile. The determination of the direction and dimension of the groundwater seepage is therefore necessary and useful for evaluating the performance of the EP.

5. Conclusions

The aim of this work was to gain a better understanding of the thermomechanical behaviors of super-long and large-diameter EPs under LNG tanks in terms of the heat transfer performance, temperature distribution, axial strain, and mobilized shaft resistance along the pile, as well as the pile settlement and its bearing capacity. Two EPs with lengths of 53 m and diameters of 1.2 m were selected for testing: EP1 was subjected to heating and static loads, and EP2 was subjected to cooling and static loads.

The comparison of the findings of previous studies with the results of the pile heating and cooling in this work showed that super-long and large-diameter EPs have better heat transfer performances: The heat flux of EP1 was 9.5 kW, the heat transfer rate was 178.3 W/m, and those of EP2 were 4.8 kW and 91.1 W/m, respectively. The temperature distributions within the two EPs showed that, overall, the temperatures in the mid-depth of the pile increased or decreased

Table 1: Comparison of heat transfer performances for different types of energy piles.

Reference	Tube configuration		Pile type (diameter/length; m)	Ground condition	Groundwater condition	Testing conditions (temperature/flow rate)	Performance (W/m)
	Radius (inner/outer; mm)	Shape					
Gao et al. [31]	20/–	1U/2U/3U/W	Concrete (0.6/25)	Sandy silt	N.A.	Constant inlet temperature (35°C/0.342 m^3/hr)	58/89/108/83
Jalaluddin et al. [32]	(40/48)/(26/33)/(20/25)	1U/2U/multi-U	Steel (0.1398/20)	Clay/sand and sandy clay	N.A.	Constant inlet temperature (27°C/4 L/min)	30.4/49.6/34.8
Zarrella et al. [33]	16/20	3U/coil (75/150/350 mm pitch)	Concrete (0.5/12)	N.A.	N.A.	Constant inlet temperature (–/0.09 kg/s) (simulated)	107/123/120/113
Yoon et al. [34]	16/20	W/coil (50 mm pitch)	PHC ((0.4/13.27)/(0.4/12.8))	Weathered granite soil/stiff weathered rock	4.5 m below pile top without groundwater flow	Constant inlet temperature (30°C/–)	95/120
Park et al. [35]	21/27	Coil (200/500 mm pitch)	Concrete ((1.5/14)/(1.5/12.5))	Silty sand with gravel/weathered rock/gneiss	N.A.	Constant inlet temperature ((–/20.33 L/min)/(–/29.17 L/min)) (intermittent)	285/248
This work	26/32	3U	Concrete (1.2/53)	Clayey soil/silty to gravelly sand/weathered sandstone	3.2–4.4 m below ground surface with groundwater flow	Constant inlet temperature ((38°C/1.8 m^3/hr)/(7°C/1.8 m^3/hr))	178 (heating)/91 (cooling)

rapidly, and at the two ends of the pile, the temperatures varied relatively slowly. By comparing the ε_{Obs} between the pure mechanical and coupled thermomechanical conditions, EP1 underwent predominately compressive deformation during the heating–loading process, while a certain tensile deformation was found near the pile toe of EP2 during the cooling–loading process. Moreover, for both EPs, positive shaft resistances occurred predominately under the pure mechanical and coupled thermomechanical conditions, which means that the shaft resistance was mainly governed by the mechanical load. The observed negative shaft resistances could be attributed to specific types of soils, that is, soft clayey and mucky soils, around the pile shaft, and the mechanical loads could prevent the mobilization of a negative shaft resistance. According to the test results, coupled thermomechanical loads did not have significant effects on the settlement and bearing capacity values of the two EPs, and the serviceability of the LNG tank would not be diminished.

Note that whether periodic heating and cooling associated with mechanical loading and unloading causing the fatigue failure of the EP in the long-term service is also a key subject, which will be studied in further works.

Data Availability

Data are available on request.

Additional Points

Highlights. Field-scale experiments of super-long and large-diameter energy pile under liquefied natural gas tank suffered to thermo-mechanical loads were carried out. Heat transfer performance of energy pile after heating and cooling was evaluated. Changes of observed axial strain and shaft resistance due to heating and cooling were discussed. Settlement and bearing capacity of energy piles were estimated.

Conflicts of Interest

The authors declare that they have no known competing financial interests or personal relationships that could have appeared to influence the work reported in this paper.

Acknowledgments

This work is supported by the Youth Research Fund (grant numbers: 20221602341030004, 20221602341030001) of the Institute of Foundation Engineering at the China Academy of Building Research, as well as by the Research Project (grant number: QDKY-2021-YFZX-04) of the CNOOC Gas and Power Group. The authors acknowledge three companies of Huaihe Energy, ZJJK, and HEBSC for their supports in conducting the in situ experiments.

References

[1] K. Zyka and A. Mohajerani, "Composite piles: a review," *Construction and Building Materials*, vol. 107, pp. 394–410, 2016.

[2] P. Jamsawang, D. T. Bergado, and P. Voottipruex, "Chapter 2 - Full-scale test on stiffened deep cement mixing piles including three-dimensional finite element simulation," *Ground Improvement Case Histories, Chemical, Electrokinetic, Thermal and Bioengineering*, pp. 31–77, 2015.

[3] P. Ravishankar and N. Satyam, "Finite element modelling to study soil structure interaction of asymmetrical tall building," in *Workshop of TC207 During the 18th International Conference on Soil-Mechanics and Geotechnical Engineering*, Paris, Report No: IIIT/TR/2013/-1, 2013.

[4] P. Badry and N. Satyam, "Seismic soil structure interaction analysis for asymmetrical buildings supported on piled raft for the 2015 Nepal earthquake," *Journal of Asian Earth Sciences*, vol. 133, pp. 102–113, 2017.

[5] H. Brandl, "Energy foundations and other thermo-active ground structures," *Geotechnique*, vol. 56, no. 2, pp. 81–122, 2006.

[6] L. Laloui, M. Nuth, and L. Vulliet, "Experimental and numerical investigations of the behavior of a heat exchanger pile," *International Journal for Numerical and Analytical Methods in Geomechanics*, vol. 30, pp. 763–781, 2006.

[7] P. J. Bourne-Webb, B. Amatya, K. Soga, T. Amis, C. Davidson, and P. Payne, "Energy pile test at Lambeth College, London: geotechnical and thermodynamic aspects of pile response to heat cycles," *Geotechnique*, vol. 59, no. 3, pp. 237–248, 2009.

[8] B. L. Amatya, K. Soga, P. J. Bourne-Webb, T. Amis, and L. Laloui, "Thermo-mechanical behavior of energy piles," *Geotechnique*, vol. 62, no. 6, pp. 503–519, 2012.

[9] K. D. Murphy and J. S. McCartney, "Seasonal response of energy foundations during building operation," *Geotechnical and Geological Engineering*, vol. 33, no. 2, pp. 343–356, 2015.

[10] K. D. Murphy, J. S. McCartney, and K. S. Henry, "Evaluation of thermo-mechanical and thermal behavior of full-scale energy foundations," *Acta Geotechnica*, vol. 10, no. 2, pp. 179–195, 2015.

[11] M. Sutman, C. G. Olgun, and T. Brettmann, "Full-scale field testing of energy piles," in *Proceeding of International Foundation Congress and Equipment Expo (IFCEE) 2015*, pp. 1638–1647, 2015.

[12] T. Mimouni and L. Laloui, "Behavior of a group of energy piles," *Canadian Geotechnical Journal*, vol. 52, no. 12, pp. 1913–1929, 2015.

[13] B. Wang, A. Bouazza, R. M. Singh, C. Haberfield, D. Barry-Macaulay, and S. Baycan, "Posttemperature effects on shaft capacity of a full-scale geothermal energy pile," *Journal of Geotechnical and Geoenviromental Engineering*, vol. 141, no. 4, Article ID 04014125, 2015.

[14] S. Q. Gui and X. H. Cheng, "In-situ tests on structural responses of energy piles during heat exchanging process," *China Journal of Geotechnical Engineering*, vol. 36, no. 6, pp. 1087–1094, (in Chinese), 2014.

[15] S. You, X. Cheng, H. Guo, and Z. Yao, "Experimental study on structural response of CFG energy piles," *Applied Thermal Engineering*, vol. 96, pp. 640–651, 2016.

[16] A. Di Donna, A. F. Rotta Loria, and L. Laloui, "Numerical study of the response of a group of energy piles under different combinations of thermo-mechanical loads," *Computers and Geotechnics*, vol. 72, pp. 126–142, 2016.

[17] H. W. Lu, G. Jiang, H. Wang et al., "In-situ tests and thermo-mechanical bearing characteristics of friction geothermal energy piles," *Chinese Journal of Geotechnical Engineering*, vol. 39, no. 2, pp. 334–342, (in Chinese), 2017.

[18] M. Faizal, A. Bouazza, C. Haberfield, and J. S. McCartney, "Axial and radial thermal responses of a field-scale energy pile

under monotonic and cyclic temperature changes," *Journal of Geotechnical and Geoenviromental Engineering*, vol. 144, no. 10, Article ID 04018072, 2018.

[19] F. Loveridge, J. S. McCartney, G. A. Narsilio, and M. Sanchez, "Energy geostructures: a review of analysis approaches, in situ testing and model scale experiments," *Geomechanics for Energy and the Environment*, vol. 22, Article ID 100173, 2020.

[20] G. Jiang, C. Lin, D. Shao et al., "Thermo-mechanical behavior of driven energy piles from full-scale load tests," *Energy and Buildings*, vol. 233, Article ID 110668, 2021.

[21] P. F. Fang, R. H. Zhang, Y. Lou et al., "Technology and application of static drilling rooted geothermal energy pile," *Journal of Shenzhen University Science and Engineering*, vol. 39, no. 1, pp. 101–109, (in Chinese), 2022.

[22] A. Kalantidou, A. M. Tang, J.-M. Pereira, and G. Hassen, "Preliminary study on the mechanical behaviour of heat exchanger pile in physical model," *Geotechnique*, vol. 62, no. 11, pp. 1047–1051, 2012.

[23] M. A. Stewart and J. S. McCartney, "Centrifuge modeling of soil–structure interaction in energy foundations," *Journal of Geotechnical and Geoenviromental Engineering*, vol. 140, no. 4, Article ID 04013044, 2014.

[24] C. W. W. Ng, C. Shi, A. Gunawan, and L. Laloui, "Centrifuge modelling of energy piles subjected to heating and cooling cycles in clay," *Geotechnique Letters*, vol. 4, no. 4, pp. 310–316, 2014.

[25] C. W. W. Ng, C. Shi, A. Gunawan, L. Laloui, and H. L. Liu, "Centrifuge modelling of heating effects on energy pile performance in saturated sand," *Canadian Geotechnical Journal*, vol. 52, no. 8, pp. 1045–1057, 2015.

[26] M. E. Suryatriyastuti, H. Mroueh, and S. Burlon, "Understanding the temperature-induced mechanical behaviour of energy pile foundations," *Renewable and Sustainable Energy Reviews*, vol. 16, no. 5, pp. 3344–3354, 2012.

[27] A. Di Donna and L. Laloui, "Numerical analysis of the geotechnical behaviour of energy piles," *International Journal for Numerical and Analytical Methods in Geomechnics*, vol. 39, no. 8, pp. 861–888, 2015.

[28] A. F. Rotta Loria, A. Gunawan, C. Shi, L. Laloui, and C. W. W. Ng, "Numerical modelling of energy piles in saturated sand subjected to thermo-mechanical loads," *Geomechanics for Energy and the Environment*, vol. 1, pp. 1–15, 2015.

[29] C. G. Olgun, T. Y. Ozudogru, and C. F. Arson, "Thermo-mechanical radial expansion of heat exchanger piles and possible effects on contact pressures at pile–soil interface," *Geotechnique Letters*, vol. 4, no. 3, pp. 170–178, 2014.

[30] T. Mimouni and L. Laloui, "Towards a secure basis for the design of geothermal piles," *Acta Geotechnica*, vol. 9, no. 3, pp. 355–366, 2014.

[31] J. Gao, X. Zhang, J. Liu, K. S. Li, and J. Yang, "Thermal performance and ground temperature of vertical pile-foundation heat exchangers: a case study," *Applied Thermal Engineering*, vol. 28, no. 17-18, pp. 2295–2304, 2008.

[32] Jalaluddin, A. Miyara, K. Tsubaki, S. Inoue, and K. Yoshida, "Experimental study of several types of ground heat exchanger using a steel pile foundation," *Renewable Energy*, vol. 36, no. 2, pp. 764–771, 2011.

[33] A. Zarrella, M. De Carli, and A. Galgaro, "Thermal performance of two types of energy foundation pile: helical pipe and triple U-tube," *Applied Thermal Engineering*, vol. 61, no. 2, pp. 301–310, 2013.

[34] S. Yoon, S.-R. Lee, J. Xue, K. Zosseder, G.-H. Go, and H. Park, "Evaluation of the thermal efficiency and a cost analysis of different types of ground heat exchangers in energy piles," *Energy Conversion and Management*, vol. 105, pp. 393–402, 2015.

[35] S. Park, D. Lee, H.-J. Choi, K. Jung, and H. Choi, "Relative constructability and thermal performance of cast-in-place concrete energy pile: coil-type GHEX (ground heat exchanger)," *Energy*, vol. 81, pp. 56–66, 2015.

[36] J. Xie and Y. Qin, "Heat transfer and bearing characteristics of energy piles: review," *Energies*, vol. 14, no. 20, Article ID 6483, 2021.

[37] China Industry Standard, *Technical Code for Testing of Building Foundation Piles. JGJ 106-2014*, China Building Industry Press, Beijing, China, (in Chinese), 2014.

[38] China Industry Standard, *Technical Standard for Utilization of Geothermal Energy Through Piles. JGJ/T 438-2018*, China Building Industry Press, Beijing, China, (in Chinese), 2018.